END

FILMED

DTIC

MICROCOPY RESOLUTION TEST CHART

NATIONAL BUREAU OF STANDARDS 1963 A

Report R84-920014-F

AD-A149 851

SOLUTION OF THE THREE-DIMENSIONAL NAVIER-STOKES
EQUATIONS FOR A STEADY LAMINAR HORSESHOE VORTEX FLOW

W. R. Briley, R. C. Buggeln and H. McDonald
Scientific Research Associates, Inc.
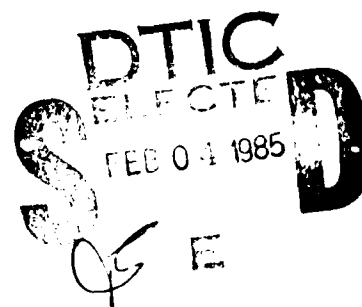P.O. Box 498
Glastonbury, CT   06033

December 1984

Final Report for Period 1 June 1982 - 30 June 1984

Approved for Public Release; Distribution Unlimited

85 01 25 057

AD-A149851

REPORT DOCUMENTATION PAGE

1a. REPORT SECURITY CLASSIFICATION	1b. RESTRICTIVE MARKINGS
Unclassified	

2a. SECURITY CLASSIFICATION AUTHORITY	3. DISTRIBUTION/AVAILABILITY OF REPORT
	Approved for Public Release;
2b. DECLASSIFICATION/DOWNGRADING SCHEDULE	Distribution Unlimited

4. PERFORMING ORGANIZATION REPORT NUMBER(S)	5. MONITORING ORGANIZATION REPORT NUMBER(S)
R84-920014-F	

6a. NAME OF PERFORMING ORGANIZATION	6b. OFFICE SYMBOL (If applicable)	7a. NAME OF MONITORING ORGANIZATION
Scientific Research Associates, Inc.		Office of Naval Research

6c. ADDRESS (City, State and ZIP Code)	7b. ADDRESS (City, State and ZIP Code)
P.O. Box 498 Glastonbury, CT 06033	800 N. Quincy Street Arlington, VA 22217

8a. NAME OF FUNDING/SPONSORING ORGANIZATION	8b. OFFICE SYMBOL (If applicable)	9. PROCUREMENT INSTRUMENT IDENTIFICATION NUMBER
		N00014-82-C-0466

8c. ADDRESS (City, State and ZIP Code)	10. SOURCE OF FUNDING NOS.			
Solution of the Three-Dimensional Navier-Stokes Equations for a Steady Laminar	PROGRAM ELEMENT NO.	PROJECT NO.	TASK NO.	WORK UNIT NO.
11. TITLE (Include Security Classification) Horseshoe Vortex Flow				

12. PERSONAL AUTHOR(S)
Briley, W.R., Buggeln, R.C., McDonald, H.

13a. TYPE OF REPORT	13b. TIME COVERED	14. DATE OF REPORT (Yr., Mo., Day)	15. PAGE COUNT
Final	FROM 82/6 TO 84/6	1984, December	43

16. SUPPLEMENTARY NOTATION

17.	COSATI CODES		18. SUBJECT TERMS (Continue on reverse if necessary and identify by block number)
FIELD	GROUP	SUB. GR.	Three-Dimensional Flow — Horseshoe Vortex Flow
			Navier-Stokes Equations — Implicit Algorithm
			Convergence Rate

19. ABSTRACT (Continue on reverse if necessary and identify by block number)

A low Mach number formulation of the three-dimensional Navier-Stokes equations is solved for a steady laminar horseshoe vortex flow, using a time-iterative approach. A split linearized block implicit algorithm is used, with central spatial differences in a transformed coordinate system. The stability of this algorithm in three dimensions is examined for a scalar convection model problem, and results are obtained which suggest that the algorithm is both conditionally stable and rapidly convergent when nonperiodic inflow/outflow boundary conditions are used. A new form of artificial dissipation which acts along physical streamlines instead of coordinate grid lines is also tested and found to introduce less error when the local flow direction is not aligned with the computational grid. An accurate solution for a laminar horseshoe vortex flow is computed using an improved solution algorithm with small artificial dissipation. This solution does not change significantly when the mesh spacing is halved using (15 x 15 x 15) and (29 x 29 x 29) grids. Very good convergence rates were obtained, such that residuals were reduced by a factor of 10^{-2} in 30 and 60 iterations respectively, for 3,375 and 24,389 grid points.

20. DISTRIBUTION/AVAILABILITY OF ABSTRACT	21. ABSTRACT SECURITY CLASSIFICATION
UNCLASSIFIED/UNLIMITED ☐ SAME AS RPT ☒ DTIC USERS ☐	Unclassified

22a. NAME OF RESPONSIBLE INDIVIDUAL	22b. TELEPHONE NUMBER (Include Area Code)	22c. OFFICE SYMBOL

ABSTRACT

A low Mach number formulation of the three-dimensional Navier-Stokes equations is solved for a steady laminar horseshoe vortex flow, using a time-iterative approach. A split linearized block implicit algorithm is used, with central spatial differences in a transformed coordinate system. The stability of this algorithm in three dimensions is examined for a scalar convection model problem, and results are obtained which suggest that the algorithm is both conditionally stable and rapidly convergent when nonperiodic inflow/outflow boundary conditions are used. A new form of artificial dissipation which acts along physical streamlines instead of coordinate grid lines is also tested and found to introduce less error when the local flow direction is not aligned with the computational grid. An accurate solution for a laminar horseshoe vortex flow is computed using an improved solution algorithm with small artificial dissipation. This solution does not change significantly when the mesh spacing is halved using $(15 \times 15 \times 15)$ and $(29 \times 29 \times 29)$ grids. Very good convergence rates were obtained, such that residuals were reduced by a factor of 10^{-2} in 30 and 60 iterations respectively, for 3,375 and 24,389 grid points.

TABLE OF CONTENTS

INTRODUCTION

The horseshoe-vortex and associated corner flows which occur when a blunt obstruction is placed within an approaching boundary layer represent a fundamental three-dimensional viscous flow of considerable interest and importance. Examples of this type of flow include the flows near an aircraft wing/fuselage junction and near a submarine hull/sail junction. The feature common to all horseshoe (or necklace) vortex flows is that a non-uniform velocity is an approaching boundary layer meets a local region of adverse pressure gradient due to the blockage effect of the obstruction. This causes a three-dimensional boundary layer separation and the formation of one or more horseshoe vortices around the obstruction. In addition to the leading edge region, the associated corner flows downstream of the leading edge are also of interest, since they contain streamwise vortices which affect the performance of both the airfoil or strut and also other devices located downstream.

The problem of horseshoe-vortex/corner flow has been investigated previously [1-2] by numerical solution of the Navier-Stokes equations. Solutions for laminar flow past an elliptical leading edge mounted normal to a flat plate endwall have been computed for both zero and five-degree angles of incidence, with chordal Reynolds number of 400, and Mach number of 0.2. Turbulent flow cases have been computed for both unswept and 45-degree swept elliptical leading edges mounted on a flat plate, with Reynolds number of 310,000 and Mach number of 0.05. Results from these flow calculations have been reported by Briley and McDonald [1-2]. Calculations for a blunt-fin induced shock wave and boundary-layer interaction flow containing a horseshoe vortex have been reported by Hung and Kordulla [3]. Detailed experimental measurements for incompressible turbulent horseshoe vortex flows have been obtained recently by McMahon, Hubbartt and Kubendran [4] and by Moore and Forlini [5].

A major impediment to the study of this and other three-dimensional flows by solution of the Navier-Stokes equations has been the high cost (computer run time) of computing accurate solutions. The high cost is attributable to the large number of grid points inherent in three dimensions and to a loss in convergence rate associated with the use of locally refined

1

(nonuniform) grids which are necessary to define the multiple length scales present in high Reynolds number viscous flows. Another difficulty is that accuracy can be degraded by the use of artificial dissipation terms which are added to central difference approximations for convective terms. Attempts to reduce this source of error by using small amounts of dissipation have led to instability in three dimensions using the present algorithm. The present investigation was undertaken to acquire an improved understanding of the stability and accuracy of the three-dimensional ADI scheme for a scalar convection model problem, which would lead to improvements in accuracy and efficiency of the solution algorithm for the Navier-Stokes equations.

In the present report, the methods used in solving the three-dimensional Navier-Stokes equations for horseshoe vortex flows are first reviewed. The questions of stability and error due to artificial dissipation are then examined for scalar convection in three dimensions. Finally, solutions for a laminar horseshoe vortex flow are computed using an improved algorithm with reduced dissipation.

GOVERNING EQUATIONS

The three-dimensional compressible Navier-Stokes equations are solved here for low Mach number and with an assumption of constant stagnation enthalpy. For these conditions, steady flow solutions closely approximate an incompressible constant density flow (cf. Briley, McDonald and Shamroth [6]). A zonal approach is used wherein the flow is computed only in a subregion of the overall flow field, near the leading edge (Fig. 1). The form of the governing equations solved permits the use of general nonorthogonal body-fitted coordinate systems, and is obtained by a transformation from Cartesian to general nonorthogonal coordinates. The Cartesian velocity components u_i and density ρ are retained as dependent variables in the transformed system of equations. The pressure, temperature and stagnation enthalpy are denoted p, T and h_o, respectively.

All variables are nondimensional in the present formulation, having been normalized by reference quantities denoted by a subscript 'r'. The quantities ρ_r, U_r, T_r amd L_r denote reference values for density, velocity, temperature and length, respectively. The reference pressure,

2

enthalpy and time are taken as $\rho_r U_r^2$, $c_p T_r$ and L_r/U_r, respectively, where c_p is the specific heat at constant pressure. The specific heat ratio is γ, and $M_r = U_r/c_r$ is a reference Mach number, where c_r is the reference sound speed defined by $c_r^2 = \gamma R T_r$, and R is the gas constant. The reference Reynolds number Re is defined by $\rho_r U_r L_r/\mu_r$, where μ_r is a reference viscosity.

The transformation T from Cartesian coordinates x_i to computational coordinates y^j is given by

$$T = y^j(x_i) \qquad i,j = 1,2,3 \tag{1}$$

Spatial derivatives are transformed according to

$$\frac{\partial}{\partial x_i} = y^j_{,i} \frac{\partial}{\partial y^j} \tag{2}$$

where unless otherwise stated the summation convention is used for repeated indices, and $y^j_{,i} \equiv \partial y^j/\partial x_i$. The coordinate system is defined by specifying the Cartesian coordinates of each computational grid point. The partial derivatives $\partial x_i/\partial y^j$ of the inverse transformation $T^{-1} = x_i(y^j)$ are then computed using three-point second-order difference formulas with uniform spacing of the computational coordinates y^j. For convenience, the y^j coordinates are normalized to give a unit mesh spacing $\Delta y^j = 1$ for each coordinate. The transformation derivatives $\partial y^j/\partial x_i$ are then computed from $\partial x_i/\partial y^j$ using standard procedures for computing derivatives of inverse functions (cf. Kaplan [7]).

The transformed Navier-Stokes equations can be written in the following nondimensional form: The continuity equation is

$$\frac{\partial \rho}{\partial t} + y^j_{,i} \frac{\partial}{\partial y^j} \rho u_i = 0 \tag{3}$$

The kth component of the momentum equation is given by

$$\frac{\partial(\rho u_k)}{\partial t} + y^j_{,1} \frac{\partial}{\partial y^j} (\rho u_1 u_k + \delta_{1k} p - \tau_{1k}) = 0 \tag{4}$$

where δ_{ik} is the Kronecker delta function. The shear stress τ_{ik} is given by

$$\tau_{1k} = Re^{-1} \left(y^m_{,k} \frac{\partial u_1}{\partial y^m} + y^m_{,1} \frac{\partial u_k}{\partial y^m} - \frac{2}{3} \delta_{1k} y^m_{,\ell} \frac{\partial u_\ell}{\partial y^m} \right) \tag{5}$$

The equation of state and definition of stagnation enthalpy can be expressed for a perfect gas as

$$p = \rho T / \gamma M_r^2 \tag{6}$$

$$h_o = T / (\gamma-1) M_r^2 + q^2/2 \tag{7}$$

where $q^2 = \delta^{ij} u_i u_j$. Although it is not necessary, it is both convenient and computationally worthwhile for the present problem to assume that h_o is a constant and to omit solution of the energy equation. This results in negligible error for steady flow at low Mach number with no heat addition. Equations (6) and (7) can then be combined to produce an adiabatic equation of state

$$p = \rho(h_o - q^2/2) (\gamma-1)/\gamma \tag{8}$$

which is used to eliminate pressure as a dependent variable in Eq. (4).

METHOD OF SOLUTION

The basic algorithm considered here has been described by Briley and McDonald [8, 9] and employs a formal time linearization to produce a noniterative fully-coupled approximation for nonlinear systems of equations, which is solved in block-implicit form using an ADI scheme with consistent intermediate steps. For a linear scalar diffusion equation, this algorithm reduces to a classical ADI scheme considered by Douglas and Gunn [10]. Warming and Beam [11, 12] have introduced a very concise derivation of this same algorithm using approximate factorization of the linearized approximation written in 'delta' form. The works of Pulliam and Steger [13], Thomas and Lombard [14] and Shamroth, McDonald and Briley [15] are representative of numerous investigations which have employed this basic algorithm.

Linearization and Time Differencing

The nonlinear system of governing equations is first written (at a single grid point) in the following form:

$$\partial H(\phi)/\partial t = D(\phi) + S(\phi) \tag{9}$$

where ϕ is the column-vector of dependent variables, H and S are column-vector algebraic functions of ϕ, and D is a column vector whose elements are the spatial differential operators which generate all spatial derivatives appearing in the governing equation associated with that element.

The solution procedure is based on the following two-level implicit time-difference approximation of (9):

$$(H^{n+1} - H^n)/\Delta t = \beta(D^{n+1} + S^{n+1}) + (1-\beta)(D^n + S^n) \tag{10}$$

where, for example, H^{n+1} denotes $H(\phi^{n+1})$ and $\Delta t = t^{n+1} - t^n$. The parameter β ($0.5 \leq \beta \leq 1$) permits a variable time-centering of the scheme, with a truncation error of order $[\Delta t^2, (\beta - 1/2 \Delta t)]$.

A local time linearization (Taylor expansion about ϕ^n) of requisite formal accuracy is introduced, and this serves to define a linear differential operator L such that

$$D^{n+1} = D^n + L^n (\phi^{n+1} - \phi^n) + 0 (\Delta t^2) \qquad (11a)$$

Similarly,

$$H^{n+1} = H^n + (\partial H/\partial\phi)^n (\phi^{n+1} - \phi^n) + 0 (\Delta t^2) \qquad (11b)$$

$$S^{n+1} = S^n + (\partial S/\partial\phi)^n (\phi^{n+1} - \phi^n) + 0 (\Delta t^2) \qquad (11c)$$

Equations (11a-c) are inserted into Eq. (10) to obtain the following system which is linear in ϕ^{n+1}

$$(A - \beta\Delta t \, L^n) (\phi^{n+1} - \phi^n) = \Delta t (D^n + S^n) \qquad (12)$$

and which is termed a linearized block implicit (LBI) scheme. Here, A denotes a square matrix defined by

$$A \equiv (\partial H/\partial\phi)^n - \beta\Delta t (\partial S/\partial\phi)^n \qquad (13)$$

Equation (12) has $0 (\Delta t)$ accuracy unless $H \equiv \phi$, in which case the accuracy is the same as Eq. (10).

Special Treatment of Diffusive Terms

Spatial cross-derivatives are present in viscous terms and in added artificial dissipation terms of the present formulation, and these cross derivative terms are evaluated explicitly at t^n. To preserve notational simplicity, it is understood that all cross-derivative terms appearing in L^n are neglected but are retained in D^n. In addition, although diffusion coefficients in viscous and dissipation terms are generally functions of the dependent variables, these coefficients are not linearized and instead are evaluated implicitly at t^n during each time step. Notationally, this is equivalent to neglecting derivatives of these coefficients with respect to ϕ

6

in L^n, which are formally present in the Taylor expansion (11a), but otherwise retaining all terms in both L^n and D^n.

It is important to note that neglecting terms in L^n has no effect on steady solutions of Eq. (12), since $\phi^{n+1} - \phi^n \equiv 0$ and thus Eq. (12) reduces to the steady form of the equations: $D^n + S^n = 0$. Aside from stability considerations, the only effect of neglecting terms in L^n is to introduce an $0(\Delta t)$ truncation error.

Consistent Splitting of the LBI Scheme

To obtain an efficient algorithm, the linearized system (12) is split using ADI techniques. To obtain the split scheme, the multidimensional operator L is rewritten as the sum of three "one-dimensional" sub-operators L_i (i = 1, 2, 3) each of which contains all terms having derivatives with respect to the i-th spatial coordinate. The split form of Eq. (12) can be derived either by following the procedure described by Douglas and Gunn in their generalization and unification of scalar ADI schemes, or using approximate factorization. In either case, for the present system of equations the split algorithm is given by

$$(A - \beta \Delta t L_1^n) \; (\phi^* - \phi^n) = \Delta t \; (D^n + S^n) \qquad (14a)$$

$$(A - \beta \Delta t L_2^n) \; (\phi^{**} - \phi^n) = A \; (\phi^* - \phi^n) \qquad (14b)$$

$$(A - \beta \Delta t L_3^n) \; (\phi^{n+1} - \phi^n) = A \; (\phi^{**} - \phi^n) \qquad (14c)$$

where $\phi*$ and $\phi**$ are consistent intermediate solutions. If spatial derivatives appearing in L_i and D are replaced by three-point difference formulas, then each step in Eqs. (14a–c) can be solved by a block-tridiagonal elimination.

Combining Eqs. (14a–c) gives

$$(A - \beta \Delta t L_1^n) \; A^{-1} \; (A - \beta \Delta t L_2^n) \; A^{-1} \; (A - \beta \Delta t L_3^n) \; (\phi^{n+1} - \phi^n)$$
$$= \Delta t \; (D^n + S^n) \qquad (15)$$

which approximates the unsplit scheme (12) to $0 (\Delta t^2)$. Since the intermediate steps are also consistent approximations for Eq. (12), physical boundary conditions can be used for $\phi*$ and $\phi**$. Finally, since the L_i are homogeneous operators, it follows from Eqs. (14a-c) that steady solutions have the property that $\phi^{n+1} = \phi* = \phi** = \phi^n$ and satisfy

$$D^n + S^n = 0 \qquad (16)$$

The steady solution thus depends only on the spatial difference approximation used for (16), and does not depend on the solution algorithm itself.

STUDIES ON ACCURACY AND CONVERGENCE RATE

In practical high Reynolds number calculations using the split LBI scheme (14a-c), artificial dissipation terms are added to the central spatial difference approximations for convective terms to control numerical oscillations, stabilize the solution algorithm, and promote convergence. Although the added dissipation terms introduce a first-order spatial truncation error in steady solutions, the magnitude of this error can be controlled using adjustable dissipation parameters and is at worst comparable to that associated with two-point "upwind" differences. The increase in accuracy derived from reduced values of added dissipation has been demonstrated in two-dimensions by Shamroth, McDonald and Briley [15] in computations of viscous transonic flow past cascades of airfoils. Unfortunately, instability has been encountered in previous three-dimensional flow calculations when only small amounts of dissipation are used. This is not surprising since the Douglas-Gunn ADI (or delta-form approximate factored) scheme applied to a simple scalar convection equation with periodic boundary conditions is known to lose its unconditional stability in three dimensions. This three-dimensional convective instability has been pointed out by Warming and Beam [16], Dwoyer and Thames [17] and others. In the present section, the behavior of the ADI scheme (14a-c) applied to scalar convection in three dimensions is considered further, and a new form for the artificial dissipation terms is examined.

8

Stability Considerations

As a model problem, the following three-dimensional scalar convection equation

$$\frac{\partial \phi}{\partial t} + u \left(\frac{\partial \phi}{\partial x} + \frac{\partial \phi}{\partial y} + \frac{\partial \phi}{\partial z} \right) = 0 \tag{17}$$

(constant u) is approximated on a unit cube with an equally spaced grid such that

$$x_j = j\Delta x \quad , \quad y_k = k\Delta y \quad , \quad z_\ell = \ell\Delta z \quad ; \quad j,k,\ell = 0,1,\ldots N \tag{18}$$

and with $\Delta x = \Delta y = \Delta z = h = N^{-1}$. The notation $\phi_{j,k,\ell}^n$ denotes $\phi(x_j, y_k, z_\ell, t^n)$, and one or more of these indices will often be omitted for simplicity. Equation (17) is approximated by the following ADI scheme analogous to (14a-c):

$$(1 - \beta\Delta t \, D_x) \, \Delta\phi^* = \Delta t \, (D_x + D_y + D_z) \, \phi^n \tag{19a}$$

$$(1 - \beta\Delta t \, D_y) \, \Delta\phi^{**} = \Delta\phi^* \tag{19b}$$

$$(1 - \beta\Delta t \, D_z) \, \Delta\phi = \Delta\phi^{**} \tag{19c}$$

where $\Delta\phi = \phi^{n+1} - \phi^n$ and $\Delta t = t^{n+1} - t^n$. Central spatial differences are used, so that the spatial difference operators appearing in (19a-c) are given by

$$D_x = (u/2h) \, (\phi_{j+1} - \phi_{j-1}) \tag{20}$$

with analogous expressions for D_y and D_z.

To examine the stability of (19a-c) using the von Neumann method, a discrete Fourier-component solution of the form

$$\phi^n_{j,k,\ell}(\bar{\omega}) = \xi^n(\bar{\omega}) \, e^{i(\omega_1 x_j + \omega_2 y_k + \omega_3 z_\ell)} \qquad (21)$$

is substituted into (19a-c) after eliminating the intermediate solutions $\Delta\phi^*$ and $\Delta\phi^{**}$, and the amplification factor $\zeta(\Delta t, \bar{\omega}) = \phi^{n+1}/\phi^n$ is determined. Here, $\bar{\omega}$ denotes the vector of frequencies $(\omega_1, \omega_2, \omega_3)$, and $i^2 = -1$. The algorithm is stable for a given time step if for all frequencies $\bar{\omega}$ present.

$$\psi \equiv \max_{\bar{\omega}} |\zeta| \leq 1 \qquad (22)$$

To cover all possible frequencies, the algorithm must be stable for arbitrary $\bar{\omega}$ in the range

$$- \Pi/h \leq \omega_1, \omega_2, \omega_3 \leq \Pi/h \qquad (23)$$

and for these conditions, it has been found that the algorithm (19) is unconditionally unstable. However, this particular stability analysis applies rigorously only for an infinite domain with periodic initial conditions, and does not account for the influence of nonperiodic boundary conditions on a finite domain.

In the present investigation, the computation of steady solutions of the Navier-Stokes equations is of primary interest, and this invariably leads to the specification of nonperiodic boundary conditions in one or more directions. In addressing steady solutions of the scalar convection equation (17), it is natural to specify function values at inflow boundaries and to employ some form of extrapolation or one-sided differencing at outflow boundaries. Accordingly, the behavior of the algorithm is investigated for $u > 0$ and with the (implicit) boundary conditions

10

$$\phi^{n+1} = \phi_b \quad \text{at} \quad \begin{cases} x = 0 \\ y = 0 \\ z = 0 \end{cases} \tag{24a}$$

$$\delta_x^2 \phi^{n+1} = 0 \quad \text{at} \quad x = 1 \tag{24b}$$

$$\delta_y^2 \phi^{n+1} = 0 \quad \text{at} \quad y = 1 \tag{24c}$$

$$\delta_z^2 \phi^{n+1} = 0 \quad \text{at} \quad z = 1 \tag{24d}$$

where ϕ_b denotes prescribed boundary values and where

$$\delta_x^2 \phi = \phi_{j+1} - 2\phi_j + \phi_{j-1} \tag{25}$$

with analogous definitions for δ_y^2 and δ_z^2. The extrapolation outflow condition is equivalent to replacing the central difference formula for the direction normal to the outflow boundary by two-point, one-sided, differences at points adjacent to the outflow boundary.

The stability of the algorithm (19) subject to the implicit boundary conditions (24) was tested in numerical experiments using $\beta = 1.0$ and different choices of Δt, h, and initial conditions. By chosing $\phi_b = 0$ on the inflow boundaries, the exact solution of the steady difference equations is $\phi = 0$, and consequently, the value of $\phi^n_{j,k,\ell}$ also represents the error $e^n_{j,k,\ell}$ from the steady solution. The stability and degree of convergence was assessed by observing the behavior of e^n with increasing n. The L_2 norm of the error at interior grid points

$$\| e^n \| = \sum_{j,k,\ell=1}^{N-1} \left(e^n_{j,k,\ell} \right)^2 \tag{26}$$

11

was monitored as an indicator of both stability and rate of convergence to the steady solution.

In each of the cases tested, the algorithm (19) with boundary conditions (24) and with $\beta = 1.0$ was found to be stable for sufficiently small Courant number $C = u\Delta t/h$, in contrast to the unconditional instability indicated by the Fourier analysis with frequencies given by (23). For example, Fig. 2 shows the computed error behavior for 50 steps using $C = 0.8$ and the (discontinuous) initial condition

$$\phi = G(x)\ G(y)\ G(z) \tag{27a}$$

$$G(a) \equiv \begin{cases} 2a & \text{for} \quad 0 \leq a \leq 0.5 \\ 1-2a & \text{for} \quad 0.5 \leq a \leq 1 \end{cases} \tag{27b}$$

The results in Fig. 2 indicate a stable calculation with good error reduction for both $N = 10$ and $N = 50$. In another example, the amplification factor for $C = 1.02$ and $N = 10$ has a theoretical value of 1.00484 (unstable) for the frequency $\bar{\omega} = (-\pi,\ -2\pi,\ 5\pi)$. Using $C = 1.02$, $N = 10$ and the initial condition

$$\phi = G(-\pi x)\ G(-2\pi y)\ G(5\pi z) \tag{27c}$$

$$G(a) = \sin(a) + \cos(a) \tag{27d}$$

which contains only this single frequency and does not satisfy the boundary conditions, the L_2 error was reduced to less than 10^{-6} its initial value in 100 iterations. Had the theoreteical amplification factor of 1.00484 been accurate for these boundary conditions, this error would have increased by 62% in 100 iterations. The discrepancy between the instability predicted by the (periodic) Fourier analysis and the empirically observed stability is attributed to the non-periodic boundary conditions (24). Since these boundary conditions are treated implicitly, they influence the solution simultaneously at all grid points during each time step.

A heuristic treatment of non-periodic boundary conditions within the von Neuman approach can be accomplished by taking the region $(0 \leq x,\ y,\ z \leq 1)$ to be a half interval for each coordinate, with periodic extension of the (nonperiodic) solution into the full interval $(-1 \leq x,\ y,\ z, \leq 1)$. At interior grid points $(1 \leq j,\ k,\ \ell \leq N-1)$, the error $e_{j,k,\ell}$ from the steady solution can be expressed as a finite Fourier series

12

containing only sine terms (odd extension), with frequencies given by

$$\omega_1 = m_1\pi \qquad m_1 = 1,2,\ldots N-1 \qquad (28a)$$

$$\omega_2 = m_2\pi \qquad m_2 = 1,2,\ldots N-1 \qquad (28b)$$

$$\omega_3 = m_3\pi \qquad m_3 = 1,2,\ldots N-1 \qquad (28c)$$

This representation correctly satisfies the condition of zero error at inflow boundaries, but incorrectly assumes zero error at outflow boundaries. The amplification factor $\zeta(\Delta t, \bar{\omega})$ for the restricted range of frequencies (28) provides a useful estimate of the observed stability, although it is heuristic in its approach to the non-periodic boundary conditions. A numerical computation for the frequency range (28) with N = 10 indicates that the maximum $|\zeta|$ numbers for which $\omega_1 = \omega_2 = \omega_3 = \omega$, and therefore it is sufficient to consider the behavior of $\zeta(\Delta t, \omega)$ for

$$0 < \omega h < \pi \qquad (29)$$

For $\beta = 1$, this leads to the following stability condition (See Appendix A)

$$C = u\Delta t/h \leq \sqrt{3/2} \qquad (30)$$

The stability of the algorithm (19) with boundary conditions (24) was tested in numerical experiments for N = 10 with initial conditions given by

$$\phi = \sum_{j,k,\ell=1}^{N-1} \sin(j\pi x)\ \sin(k\pi y)\ \sin(\ell\pi z) \qquad (31)$$

which includes contributions of unit amplitude from all frequencies in (28). The quantity

$$\| e^{n+1} \| / \| e^n \| \qquad (32)$$

13

is taken as an empirical measure of the maximum amplification factor ψ for the purpose of assessing stability. Computed values of ψ after 30 iterations are shown in Fig. 3, along with theoretical curves for both the full range of frequencies (23) and for positive frequencies in the range

$$0 \le \omega_1, \omega_2, \omega_3 \le \pi/h \qquad (33)$$

which led to the estimate (30) for stability. The theoretical curves were obtained numerically using a sampling increment of $\pi/10h$ for each frequency. For the conditions of these test calculations, the stability condition (30) provides a useful and somewhat conservative estimate of the observed limit of stability. Although the present results provide only a limited model for the Navier-Stokes equations, the stability and rapid convergence rates obtained here with proper time step selection are very encouraging. It is later demonstrated here that rapid convergence can also be obtained for the three-dimensional Navier-Stokes equations with small values of artificial dissipation.

Second-Order Artificial Dissipation

One method of adding dissipation is equivalent to a replacement of the convective derivative operator for each coordinate direction by a modified operator, as follows:

$$u \frac{\partial}{\partial x} \leftarrow u \frac{\partial}{\partial x} - \sigma \frac{|u| \Delta x}{2} \frac{\partial^2}{\partial x^2} \qquad (34)$$

with analogous replacements for $v \partial(\ )/\partial y$ and $w \partial(\ )/\partial z$. When three-point central differences are used on a uniform grid, the resulting approximation is equivalent to the two-point upwind difference scheme when $\sigma = 1$. This latter scheme has first-order accuracy and is especially inaccurate when the velocity is not aligned with the computational grid. Alternatives to this upwind scheme have received considerable attention (see, for example, Raithby [18], Baliga and Patankar [19], and Brooks and Hughes [20]). A very simple but effective method of improving the accuracy of the upwind scheme is to express the scheme in terms of central differences and an added dissipation as in (34) and then reduce the dissipation parameter σ. For sufficiently small values of σ, this method obviously approaches the accuracy

14

of the second-order central difference scheme. Dissipation of the form given
in (34) will be referred to here as 'upwind' dissipation.

When the velocity is not aligned with the coordinate mesh, the accuracy
for a given value of σ can be improved by adopting a different form for the
dissipation terms, which acts to smooth convected quantities only in the
direction along streamlines. This form of dissiaption is used in the
streamline-upwind method of Brooks and Hughes [20] and is also present in the
tensor viscosity method of Dukowicz and Ramshaw [15]. Dissipation of this
type will be referred to here as 'streamwise' dissipation, and can be
illustrated as follows:

If s denotes distance along a streamline, and if $\bar{s}$ is the unit vector in
the direction of the streamline, then the velocity vector $\bar{U}$ can be expressed
as $\bar{U} = q\bar{s}$ where $q^2 = \bar{U} \cdot \bar{U}$, and the convective operator can be expressed as

$$\bar{U} \cdot \nabla = q \frac{\partial}{\partial s} \tag{35}$$

where

$$\frac{\partial}{\partial s} = \bar{s} \cdot \nabla \tag{36}$$

Streamwise dissipation can be added by replacing the convective operator by a
modified operator analogous to (34) as follows:

$$\bar{U} \cdot \nabla \leftarrow q \frac{\partial}{\partial s} - \sigma \frac{q\Delta s}{2} \frac{\partial^2}{\partial s^2} \tag{37}$$

where

$$(q\Delta s)^2 = (u \ \Delta x)^2 + (v \ \Delta y)^2 + (w \ \Delta z)^2 \tag{38}$$

In three dimensions and for constant velocity, the streamwise dissipation
term has the form

15

$$- \sigma \frac{\Delta s}{2q} \left[u^2 \frac{\partial^2}{\partial x^2} + v^2 \frac{\partial^2}{\partial y^2} + w^2 \frac{\partial^2}{\partial z^2} + 2uv \frac{\partial^2}{\partial x \partial y} + 2uw \frac{\partial^2}{\partial x \partial z} + 2vw \frac{\partial^2}{\partial y \partial z} \right] \quad (39)$$

The above form is equivalent to upwind dissipation only in one dimension ($u \neq 0$, $v = w = 0$) or if the mixed-derivative terms are omitted. In the numerical algorithm, the mixed derivative terms are evaluated explicitly. Warming and Beam [22] have shown for a three-dimensional scalar diffusion equation that the explicit treatment of mixed-derivative terms does not upset the unconditional stability of the ADI scheme (19) with $\beta = 1$.

The effect of upwind and streamwise dissipation on accuracy was examined for a three-dimensional test problem suggested by Abarbanel, Dwoyer and Gottlieb [23]. Here, the convection equation (17) is solved in the unit cube with equal mesh increments and for $N = 10$. An exact steady solution Φ of equation (17) for these conditions is given by

$$\Phi = \cos [2\pi(x-y)] + \cos [2\pi(y-z)] + \cos [2\pi(x-z)] \quad (40)$$

In this test problem, the velocity vector is directed diagonally to each incremental mesh cube. In the present calculations, the correct boundary conditions for ϕ were prescribed from this known exact solution ($\phi = \Phi$ at inflow; $\delta^2 \phi = \delta^2 \Phi$ at outflow). It was noted that the central difference scheme without dissipation ($\sigma = 0$) reproduced the exact solution Φ at all grid points. Consequently, the error $\phi - \Phi$ in the present calculations is entirely due to the added dissipation. The maximum error $|\phi - \Phi|/(\Phi_{max} - \Phi_{min})$ at interior points is shown in Fig. 4 as a function of the dissipation parameter σ for both the upwind (34) and streamwise (39) forms of dissipation. Although the coarse mesh used ($N = 10$) causes relatively large errors at large values of σ, the streamwise dissipation (39) provides a considerable improvement in accuracy for a given value of σ. Other solutions were computed in which resolution was improved by using the same coarse grid ($N = 10$) but for computational domains smaller than the unit cube. These results confirm that the increased accuracy of streamwise dissipation over upwind dissipation for fixed σ is maintained when the grid resolution is increased.

16

COMPUTED RESULTS FOR A LAMINAR HORSESHOE VORTEX FLOW

Flow Conditions

Solutions are presented here for laminar flow at zero incidence past an elliptical leading edge geometry mounted between parallel flat plate endwalls. The purpose of these calculations was to determine whether the improved understanding of stability and accuracy acquired in the present model problem studies could be exploited to allow computation of accurate solutions of the three-dimensional Navier-Stokes equations using the split LBI scheme with small amounts of artificial dissipation. The leading-edge geometry for the present calculations is the same as that considered by McMahon, Hubbartt and Kubendran [4] for turbulent flow conditions. A laminar flow case was chosen here to allow an accurate assessment of the numerical method, which is not clouded by extraneous factors associated with turbulence modelling. The computation of turbulent flow cases will be undertaken in a future investigation.

The flow geometry (Fig. 1) consists of a strut of constant thickness W having an elliptical leading edge with 1.5:1 ratio of major to minor axis. The strut is mounted normal to parallel flat plate endwalls whose separation distance is 5.0W, and whose leading edges are located a distance 6.0W upstream of the leading edge of the strut. The length L of the strut within the computational domain is 2.5W. The flow considered has a Reynolds number Re = 200 (based on L) and Mach number M_r = 0.1, each based on upstream flow conditions.

Boundary Conditions

Since the computational domain is chosen to be a region in the immediate vicinity of the leading-edge/corner flow geometry (cf. Fig. 1) embedded within a larger overall flow system, inflow and outflow boundary conditions which adequately model the interface between the computed flow and the remainder of the flow system are required. The inflow/outflow conditions used are derived from an assumed flow structure and are chosen to provide inflow with prescribed stagnation pressure (and stagnation enthalpy) in an inviscid core region and with a given axial velocity profile shape in the

17

endwall boundary layer, and to provide outflow with a prescribed distribution of static pressure in the cross section. This approach to inflow/outflow boundary conditions has been discussed previously in [1-2] and is only summarized here.

First, the boundary layer thickness $\delta(x_1)$ on the endwall flat plate is approximated by its distribution from the Blasius flat plate solution. At the inflow boundary, a "two-layer" boundary condition is employed such that stagnation pressure p_o is fixed at the free stream reference value in the core flow region $(y^3 > \delta)$ and an axial velocity profile shape $u_1/u_e = f(y^3/\delta)$ is fixed within the boundary layer region $(y^3 \leq \delta)$. Here, u_e is the local edge velocity which varies with time and is adjusted after each time step to the value consistent with p_o and the local edge static pressure, which is determined as part of the solution. The remaining inflow conditions are $u_2 = \partial^2 u_3/\partial n^2 = \partial^2 p/\partial n^2 = 0$, where n denotes the normal computational coordinate, y^1. For outflow conditions, a constant static pressure is imposed, and second derivatives of each velocity component are set to zero. At no-slip surfaces, each velocity component u_i is set to zero, and the remaining condition applied to these surfaces is that the derivative of pressure in the direction normal to the surface is zero. This condition approximates the normal momentum equation to order Re^{-1} for viscous flow at a no-slip surface. The final boundary to be considered is the plane parallel to the endwall and in the free stream. This boundary is assumed to be a plane of symmetry, so that the flow represented is that past the strut mounted between parallel flat plates.

Computational Details

For constant stagnation enthalpy, the governing equations consist of continuity (3) and three components of momentum (4). After eliminating pressure using (8), these equations are solved using the split LBI scheme (14), linearized with respect to the dependent variables $\phi^T = (\rho, u_1, u_2, u_3)$. Central spatial differences are used on an equally spaced grid for each transformed coordinate y^j, and streamwise dissipation terms analogous to (39) are added to these equations.

For each governing equation, the streamwise dissipation term can be expressed as

$$\frac{\sigma \rho^k Q}{2} s^j s^k \frac{\partial^2 \psi}{\partial y^j \partial y^k} \qquad (41)$$

where $s^j = U^j/Q$ are components of a unit vector, and where

$$U^j = y^j_{,i} u_i \qquad (42a)$$

$$Q^2 = U^j U^k \delta_{jk} \qquad (42b)$$

Here, σ is a dissipation parameter, ψ is a scalar representing the appropriate dependent variable (ρ for continuity and u_k for the kth momentum equation), and k is 0 for continuity but otherwise 1.

The quantity V defined by

$$V^2 = \left(f^j s^k \right)^2 \delta_{jk} \qquad (43)$$

where

$$f^j = Re^{-1} \sum_i \left(y^j_{,i} \right)^2 \qquad (44)$$

is a measure of the physical diffusion in the streamwise direction. The artificial dissipation term (41) is omitted at points for which V is greater than $\sigma \rho^k Q/2$. In the present calculations, the value $\sigma = 0.1$ was used for the dissipation parameter. It should be recalled that for scalar convection in one dimension, the value $\sigma = 1.0$ is equivalent to two-point upwind differencing, and thus the value $\sigma = 0.1$ is relatively small.

Although a uniform grid was used for the transformed coordinates y^j, the grid used is highly nonuniform in physical coordinates x_i, as shown in Fig. 1, and was chosen to provide resolution of several length scales known to be present for this type of flow. Care was taken to provide resolution of the boundary layers on the strut and endwall surfaces, of the shear layer near the leading-edge stagnation line, and of the corner flow region very near the endwall/leading-edge intersection. Two computational grids,

19

consisting of 15 and 29 equally spaced points for each transformed coordinate direction, were used to compute solutions which were otherwise identical. For the finer grid, the mesh spacings adjacent to the endwall and strut surfaces were 0.0005W and 0.0085W, respectively.

A pseudo-time dependent iteration procedure was employed in which the square matrix A in the LBI scheme (14) is replaced by a modified matrix A + AB, where B is a diagonal conditioning matrix. This technique was employed by Briley, McDonald and Shamroth [6] to improve the convergence rate of this algorithm when applied to low Mach number flows. In the present calculations, a diagonal matrix B whose diagonal elements are $(1/\gamma M_r^2, 1, 1, 1)$ was used. In addition, a spatially varying time step was used to avoid instability analogous to that encountered for the three-dimensional scalar convection equation, and to improve the convergence rate. Several procedures for time step selection for the Navier-Stokes equations are presently under investigation, and the present results should be taken ony as a demonstration that this technique can provide a good rate of convergence to the steady solution. A more detailed account of variuos techniques for time step selection will be given in a forthcoming paper.

Computed Results

Before proceeding to a discussion of the horseshoe vortex flow, an indication is given of the degree and rate of convergence obtained for these three-dimensional calculations, and of the effect of halving the mesh on the computed solutions. The convergence rate for each of the two grids is shown in Fig. 5, where the maximum residual in the field is normalized by its value at the start of the calculation. A very good rate of convergence was obtained for a relatively small value of dissipation parameter ($\sigma = 0.1$). Reducing the normalized residuals to 10^{-2} gave convergence to within a tolerance not distinguishable in the plots of computed flow variables given here, and this required about 30 to 60 iterations, respectively, for the (15 x 15 x 15) and (29 x 29 x29) grids.

The effect of halving the mesh spacing on the computed distributions of flow variables at a representative location is shown in Fig. 6. The distributions of each velocity component and static pressure coefficient $C_p = 2(p - 1/\gamma M_r^2)$ in the x3 direction are given for a line normal to the

endwall and within the plane of symmetry upstream of the strut leading edge, located a distance 0.22W upstream of the leading edge. This location has the peak value of reversed flow in the u_1 velocity component. The comparison in Fig. 6 is representative of that found throughout the flow field. The solution does not change significantly when the mesh is halved, and this is an indication that the solutions are accurate and that the flow behavior is adequately resolved using these grids. The sensitivity of the coarse mesh solution to the location of the outflow boundary was also tested by adding grid points to move the outflow boundary downstream a distance 6.1W, and this had no significant affect on the solution.

Computed results for the (29 x 29 x 29) grid are shown in a series of plots in Figs. 7, 8 and 9a-f. In Fig. 7, velocity vector plots in the plane of grid points adjacent to the no-slip endwall surface are contrasted with corresponding results from the symmetry plane midway between the endwalls. The vector magnitudes are renormalized for each plot and thus indicate only flow direction and relative magnitude within the plot. A reversed flow region within the horseshoe vortex is clearly visible near the endwall. The reversed flow region includes two saddle-point flow separations associated with the horseshoe vortex flow structure. One of the saddle points is very close to the leading edge and is not clearly visible in Fig. 7.

The computed flow behavior in the corner region near the intersection of the strut and endwall is shown in Figs. 8-9. The flow is shown in planes normal to the strut surface and intersecting the endwall, as indicated in Fig. 8. Vector plots of velocity within these planes and contour plots of normal velocity, static pressure coefficient C_p and total pressure coefficient C_{po} are shown in Figs. 9a-f. The cross sections have a width of 2W and height of 1.25W. The horseshoe vortex formation in the stagnation symmetry plane (plane 1) can be seen in Fig. 9a. There is a strong downward velocity toward the endwall in the region near the leading edge (behind the saddle-point separation), with maximum downward velocity about 45 per cent of the free stream reference velocity. The maximum reversed flow velocity (u_1) is about 7 per cent of the reference velocity (see also Fig. 6). The horseshoe vortex continues its development at downstream locations and moves outward away from the corner region and into the free stream. The contours of velocity normal to the cross sectional planes give an indication of the shear layer development on the strut and endwall surfaces and also show the

21

distortion of the shear layers in the corner region due to the horseshoe vortex. The static pressure field is highly three-dimensional, with significant spanwise gradients along the strut surface and low pressure near the strut/endwall intersection. Although no other analytical results or experimental measurements of the three-dimensional horseshoe vortex flow are available for comparison, the present computed results are consistent with flow visualization studies of related leading edge vortex flows.

CONCLUDING REMARKS

Significant progress has been made in improving the accuracy/convergence-rate properties of the present numerical method for the three-dimensional Navier-Stokes equations. It has been demonstrated for the laminar flow considered that an accurate (grid insensitive) steady solution can be computed and that good convergence rates can be obtained in three dimensions, using only small amounts of artificial dissipation. These calcultions were performed using locally-refined nonuniform grids of the type needed to define the multiple length scales present in high Reynolds number viscous flows. A future study will address the computation of turbulent flow cases with resolution of the viscous sublayer region. Based on our recent experience with a vectorized version of this code on a CRAY-1 computer, it should soon be possible to compute solutions for a 30 x 30 x 30 grid (27,000 points) in about 10 minutes of run time.

APPENDIX A

Under the condition that the frequencies for each coordinate direction are equal ($\omega_1 = \omega_2 = \omega_3 = \omega$), the amplification factor for the algorithm given in (19a-c) can be written in the form

$$\zeta = \frac{\alpha_1 + i\,\beta_1}{\alpha_2 + i\,\beta_2} \tag{A.1}$$

where

$$\alpha_1 = \alpha_2 = 1 - 3\,(CA)^2 \tag{A.2a}$$

$$\beta_2 = -3CA + (CA)^3 \tag{A.2b}$$

$$\beta_1 = \beta_2 + 3CA/\beta \tag{A.2c}$$

and where

$$C = u\Delta t/h \tag{A.3}$$

$$A = \beta\sin(\omega h) \tag{A.4}$$

Because $\alpha_1 = \alpha_2$, neutral stability occurs when $\beta_1 = \beta_2$, which yields

$$CA = [3(2\beta-1)/2\beta]^{1/2} \tag{A.5}$$

The maximum value of A occurs for $\omega h = \pi/2$, and this gives the following stability condition:

$$C \leq \beta^{-1}\,[3(2\beta-1)/2\beta]^{1/2} \tag{A.6}$$

The special case $\beta = 1$ gives $C \leq \sqrt{3/2}$.

REFERENCES

1. Briley, W.R. and McDonald, H.: Computation of Three-Dimensional Horseshoe Vortex Flow Using the Navier-Stokes Equations. Seventh Int. Conf. on Num. Methods in Fluid Dyn., Stanford, 1980.

2. Briley, W.R. and McDonald, H.: Computation of Turbulent Horseshoe Vortex Flow Past Swept and Unswept Leading Edges. SRA Report R82-920001-F, 1982.

3. Hung, L.M. and Kordulla, W.: A Time-Split Finite Volume Algoirthm for Three-Dimensional Flow Field Simulation, AIAA Paper 83-1957, 1983.

4. McMahon, H., Hubbartt, J. and Kubendran, L.R.: Mean Velocities and Reynolds Stresses Upstream of a Simulated Wing-Fuselage Juncture, NASA CR-3695, 1983.

5. Moore, J. and Forlini, T.J.: A Horseshoe Vortex in a Duct, J. Engr. for Gas Turbines and Power, Vol. 106, 1984, p. 668.

6. Briley, W.R., McDonald, H. and Shamroth, S.J.: A Low Mach Number Euler Formulation and Application to Time-Iterative LBI Schemes, AIAA Journal, Vol. 21, No. 10, October 1983, p. 1467.

7. Kaplan, W.: Advanced Calculus, Addison-Wesley Publishing Company, Inc., 1952.

8. Briley, W.R. and McDonald, H.: Solution of the Multidimensional Compressible Navier-Stokes Equations by a Generalized Implicit Method, J. Comp. Physics, Vol. 24, August 1977, p. 372.

9. Briley, W.R. and McDonald, H.: On the Structure and Use of Linearized Block Implicit and Related Schemes, J. Comp. Physics, Vol. 34, 1980, p. 54.

10. Douglas, J. and Gunn, J.E.: A General Formulation of Alternating Direction Methods, Numerische Math., Vol. 6, 1964, p. 428.

11. Warming, R.F. and Beam, R.M.: On the Construction and Application of Implicit Factored Schemes for Conservation Laws, Symposium on Computational Fluid Dynamics, New York, April 1977; SIAM-AMS Proceedings, Vol. 11, 1977.

12. Beam, R.M. and Warming, R.F.: An Implicit Factored Scheme for the Compressible Navier-Stokes Equations. AIAA Journal, Vol. 16, 1978, p. 393.

13. Pulliam, T.H. and Steger, J.L.: Implicit Finite Difference Simulations of Three-Dimensional Compressible Flow, AIAA Journal, Vol. 18, 1980, p. 159.

14. Thomas, P.D. and Lombard, C.K.: Geometric Conservation Law and Its Application to Flow Computations on Moving Grids, AIAA Journal, Vol. 17, 1979, p. 1030.

REFERENCES (Continued)

15. Shamroth, S.J., McDonald, H. and Briley, W.R.: Prediction of Cascade Flow Fields Using the Averaged Navier-Stokes Equations, J. Engr. for Gas Turbines and Power, 1984, Vol. 106, p. 383.

16. Warming, R.F. and Beam, R.M.: An Extension of A-Stability to Alternating Direction Implicit Methods. BIT, Vol. 19, p. 395, 1979.

17. Dwoyer, D.L. and Thames, F.C.: Accuracy and Stability of Time-Split Finite-Difference Schemes, AIAA Paper 81-1005, 1981 AIAA CFD Conference, Palo Alto, CA, 1981.

18. Raithby, G.D.: Skew Upstream Differencing Schemes for Problems Involving Fluid Flow, Comp. Meth. in Applied Mech. and Engr., Vol. 9, pp. 153-164, 1976.

19. Baliga, B.R. and Patankar, S.V.: A New Finite-Element Formulation for Convection-Diffusion Problems, Numerical Heat Transfer, Vol. 3, pp. 393-409, 1980.

20. Brooks, N. and Hughes, J.R.: Streamline Upwind/Petrov-Galerkin Formulations for Convection Dominated Flows with Particular Emphasis on the Incompressible Navier-Stokes Equations, Comp. Meth. in Appl. Mech. and Engr., Vol. 32, pp. 199-259, 1982.

21. Dukowicz, J.K. and Ramshaw, J.D.: Tensor Viscosity Method for Convection in Numerical Fluid Dynamics, J. Comp. Physics, Vol. 32, pp. 71-79, 1979.

22. Warming, R.F. and Beam, R.M.: Recent Advances in the Development of Implicit Schemes for the Equations of Fluid Dynamics, Proceedings of the Seventh Intl. Conf. on Numerical Methods in Fluid Dynamics, Springer-Verlag, p. 429, 1980.

23. Abarbanel, S.S., Dwoyer, D.L. and Gottlieb, D.: Stable Implicit Finite-Difference Methods for Three-Dimensional Hyperbolic Systems. ICASE Report 82-39, Nov. 1982.
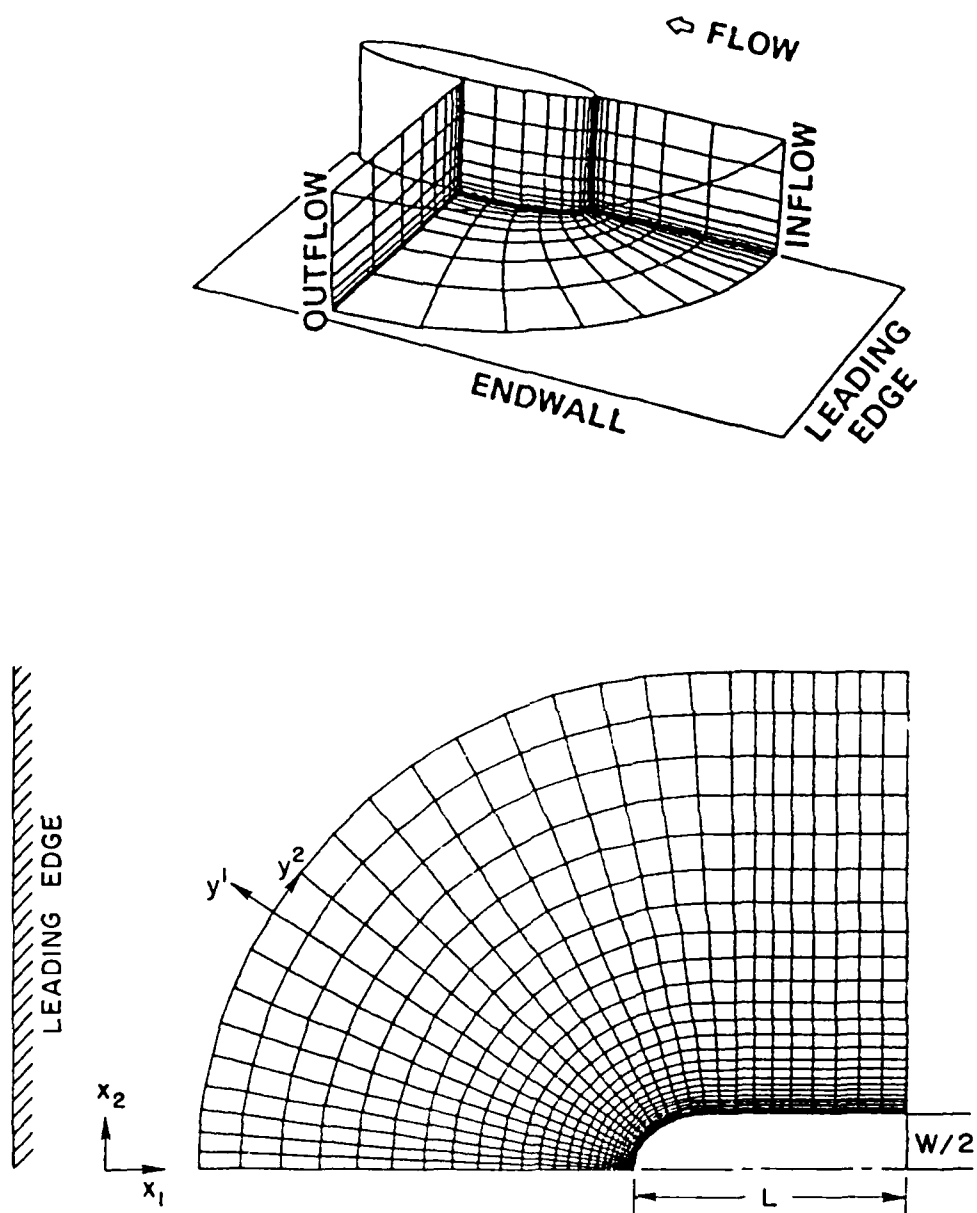
Fig. 1 - Flow Geometry and Coordinate System.
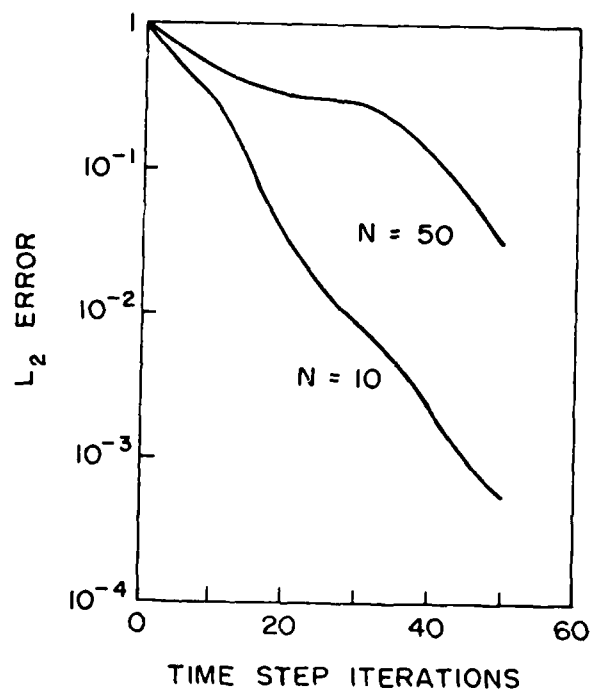
Fig. 2 - Computed Behavior of L_2 Error from Steady Solution for Scalar Convection Test Problem with $C=0.8$ and $h=N^{-1}$.
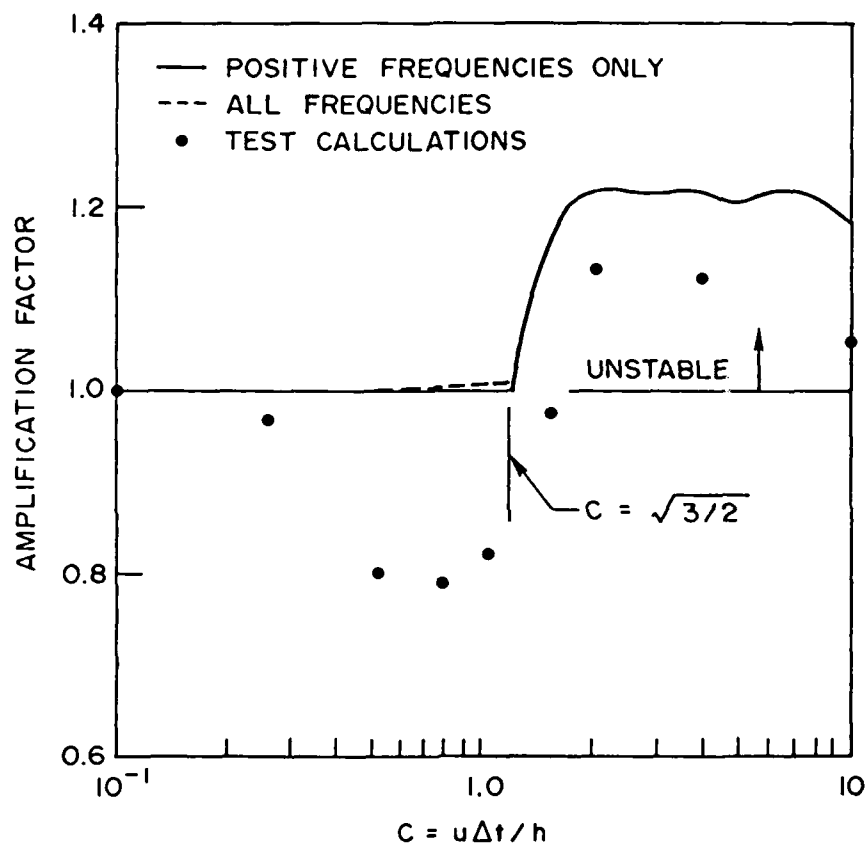
Fig. 3 – Stability Test Problem for Three-Dimensional Scalar Convection with $h=10^{-1}$.
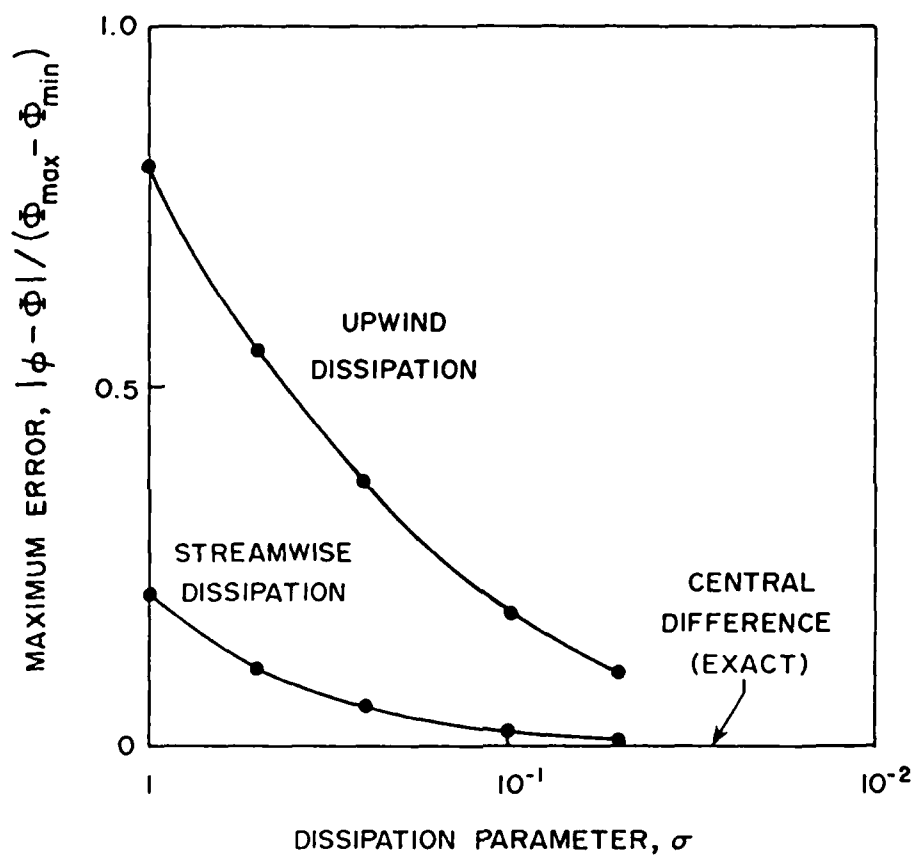
Fig. 4 – Effect of Dissipation Parameter on Error in Steady Solution for a Three-Dimensional Test Problem.

29
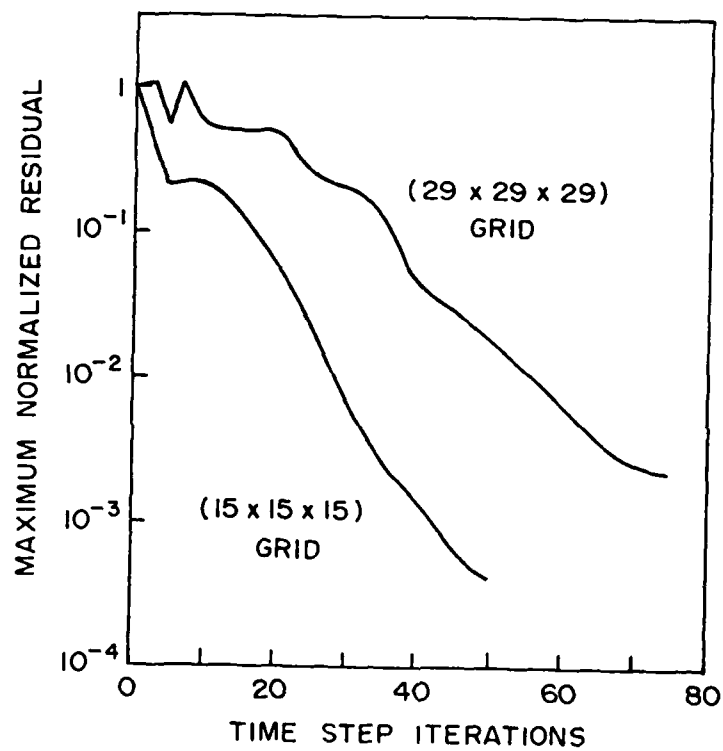
Fig. 5 – Convergence Rate for Three-Dimensional Low Mach Number
Formulation of the Navier Stokes Equations, with σ=0.1.
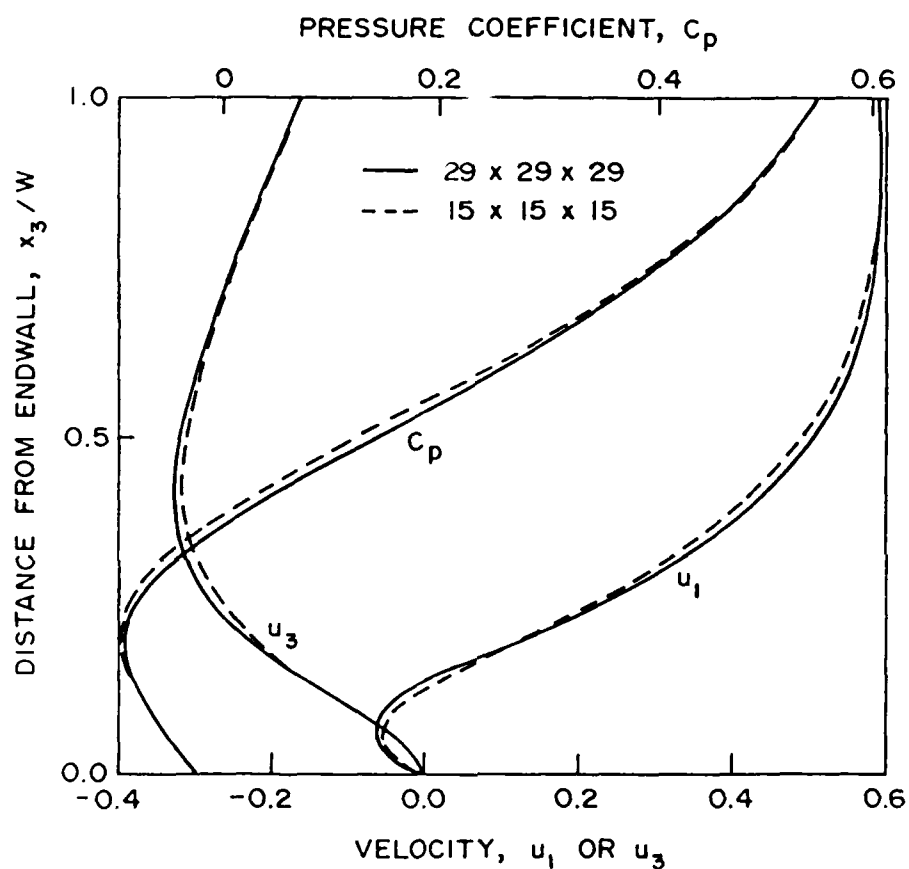
Fig. 6 – Effect of Grid on Computed Flow Distributions at a Representative Location 0.22W Upstream of the Strut Leading Edge.

31
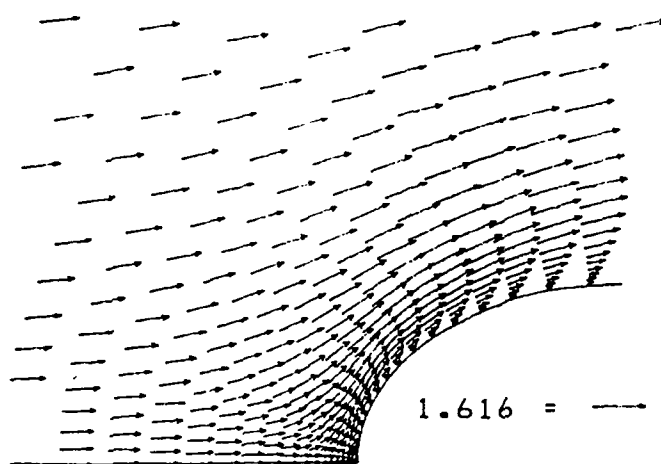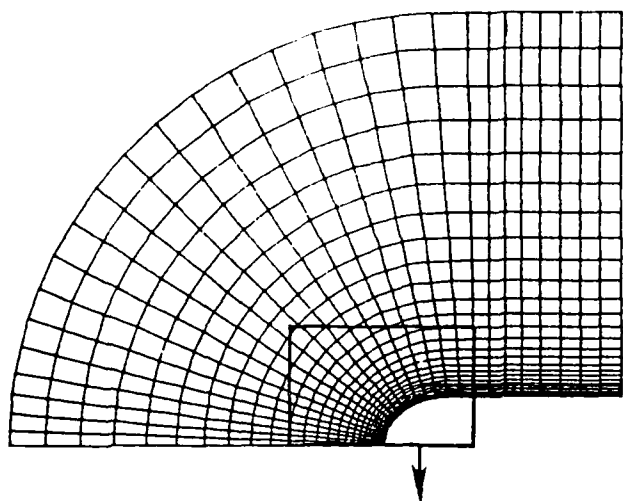
x_3 / W = 2.5

FREESTREAM
SYMMETRY
PLANE

$1.616 = \longrightarrow$
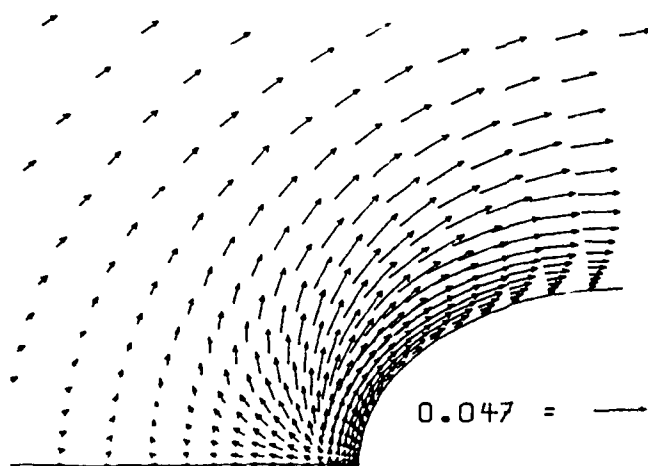
x_3 / W = 0.0005

NEAR
ENDWALL

$0.047 = \longrightarrow$

Fig. 7 - Vector Plots of Computed Velocity in Planes Parallel to the Endwall.

32
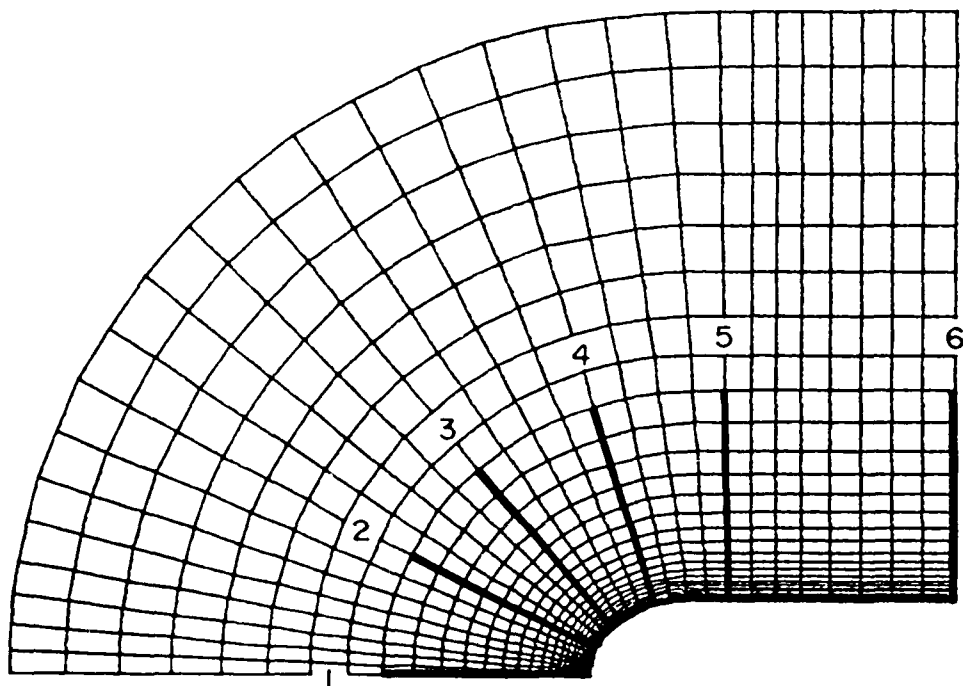
Fig. 8 - Locations of Cross Sectional Planes Normal to Strut and Endwall Surfaces.

1.231 ——

GRID

STRUT

ENDWALL

TRANSVERSE VELOCITY

.94

-.16

-.34

.02

STATIC PRESSURE COEFFICIENT

.94

.02

-.34

-.16

TOTAL PRESSURE COEFFICIENT
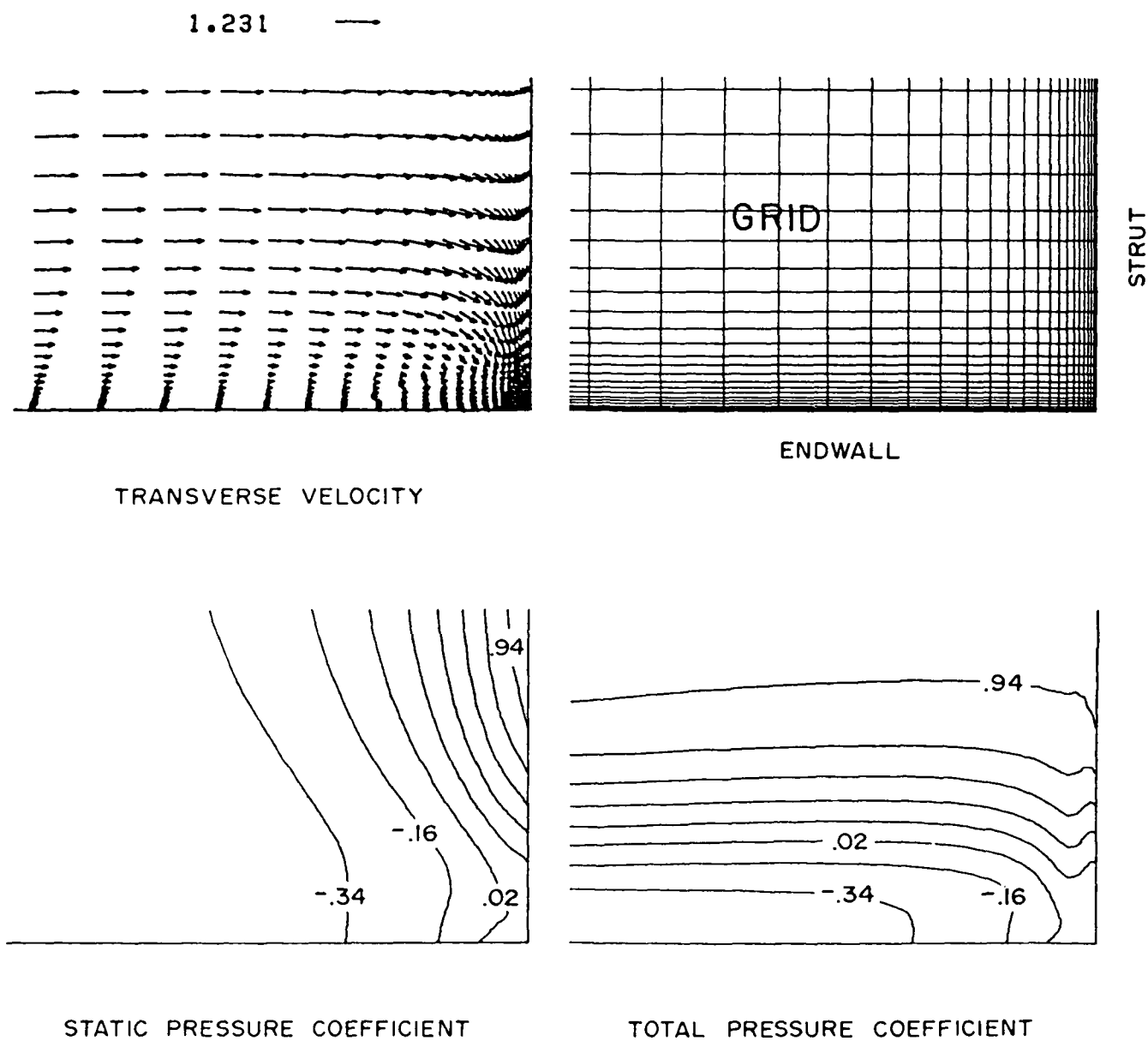
Fig. 9a – Computed Flow Variables at Plane 1.
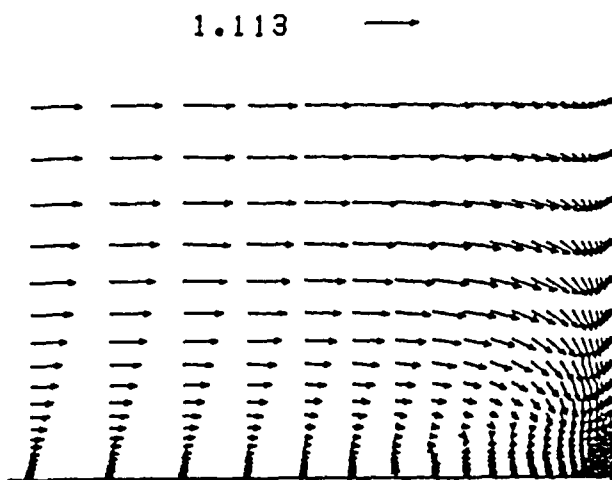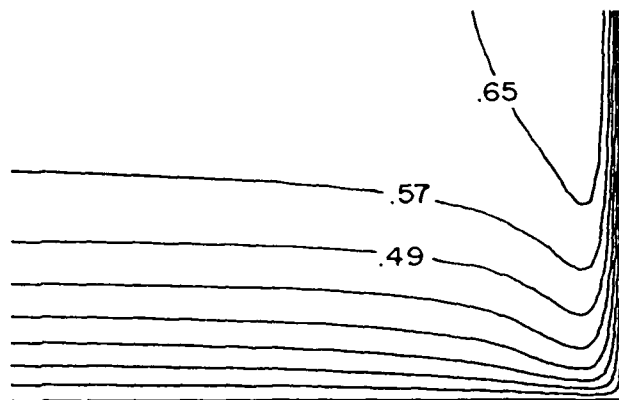
34

1.113 →

TRANSVERSE VELOCITY

NORMAL VELOCITY

.65

.57

.49

STATIC PRESSURE COEFFICIENT

.29

-.47   -.36

TOTAL PRESSURE COEFFICIENT

.83

.65

.41
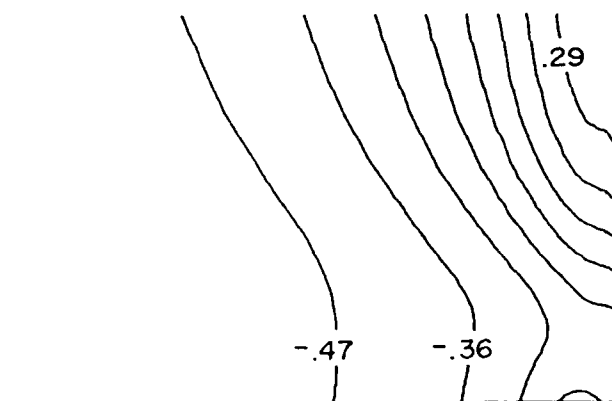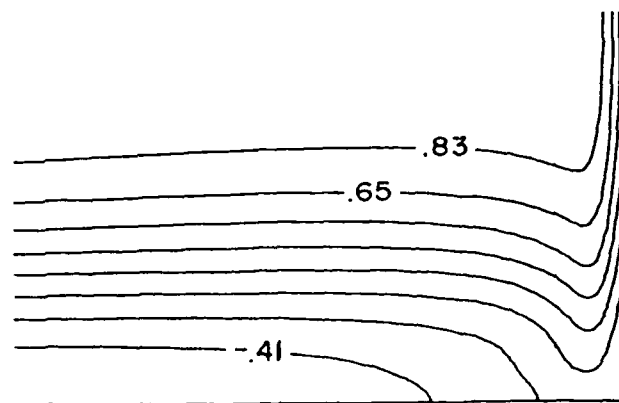
Fig. 9b – Computed Flow Variables at Plane 2.
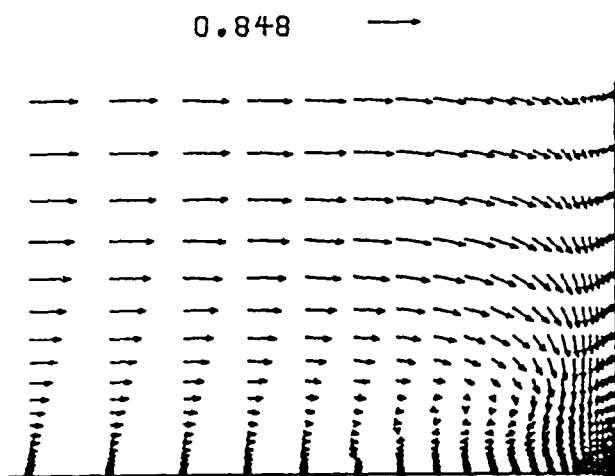
35

0.848 →

TRANSVERSE VELOCITY

NORMAL VELOCITY

1.10

.97

.83

-.52

-.62

-.67

.79

.58

-.48

-.70
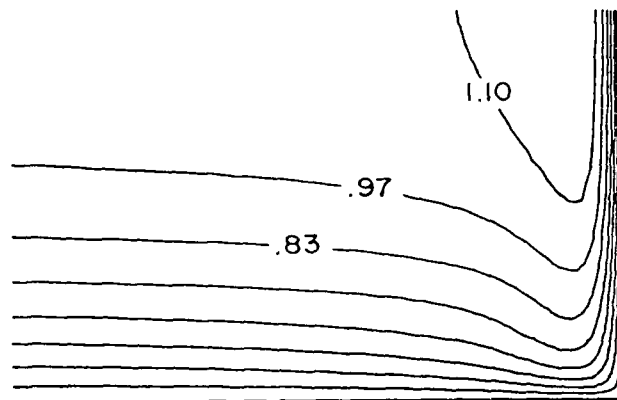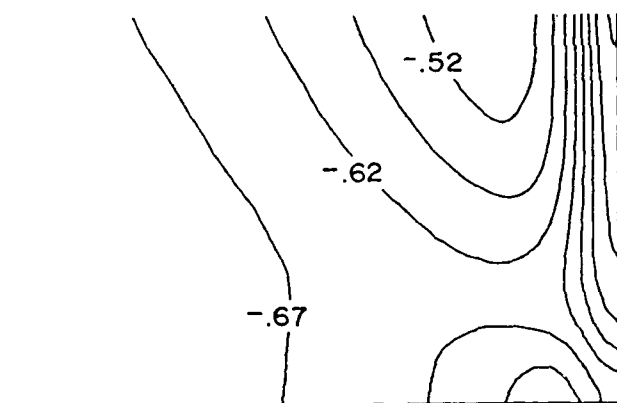
STATIC PRESSURE COEFFICIENT
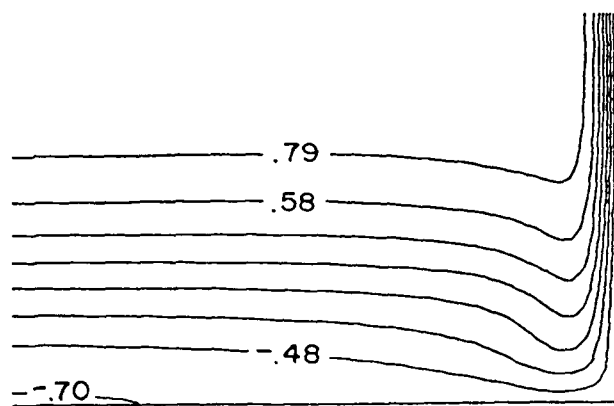
TOTAL PRESSURE COEFFICIENT

Fig. 9c – Computed Flow Variables in Plane 3.
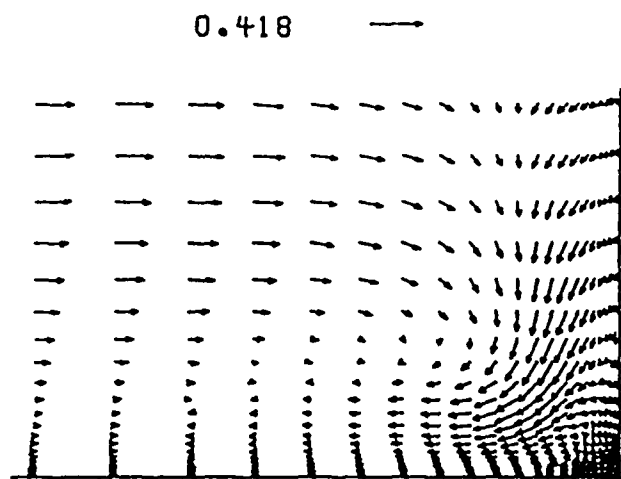
36

0.418   →

TRANSVERSE VELOCITY   NORMAL VELOCITY
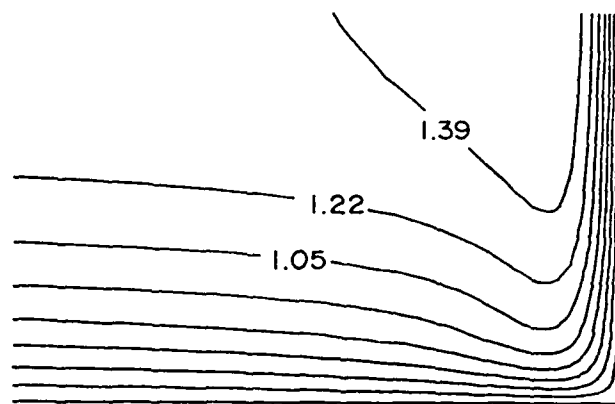
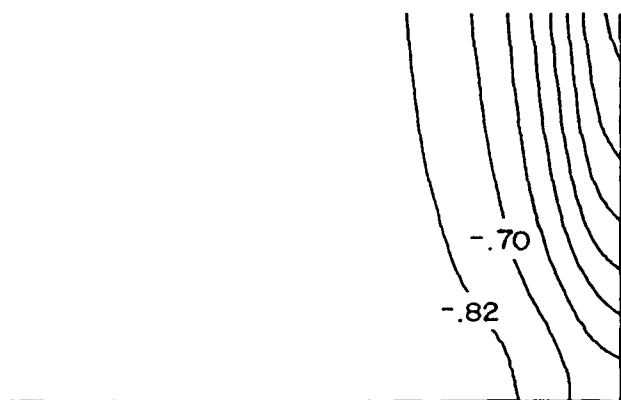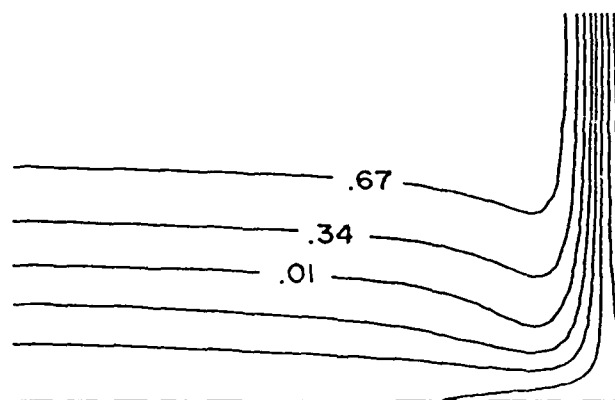STATIC PRESSURE COEFFICIENT   TOTAL PRESSURE COEFFICIENT

Fig. 9d – Computed Flow Variables in Plane 4.

37

0.256 ⟶

TRANSVERSE VELOCITY

NORMAL VELOCITY

STATIC PRESSURE COEFFICIENT

TOTAL PRESSURE COEFFICIENT

Fig. 9e – Computed Flow Variables in Plane 5.

38

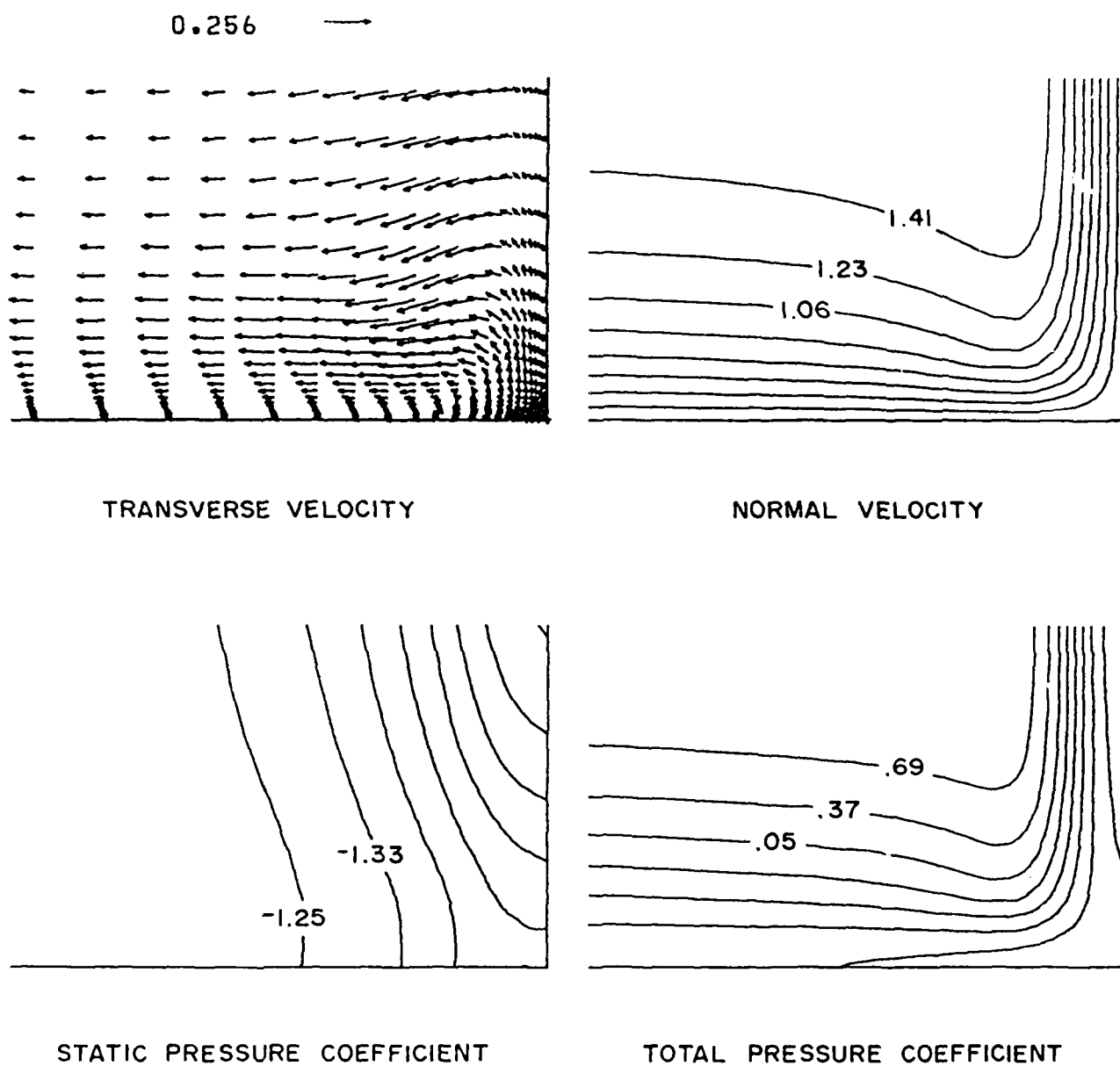0.147 ⟶

TRANSVERSE VELOCITY

NORMAL VELOCITY

CONSTANT C_p

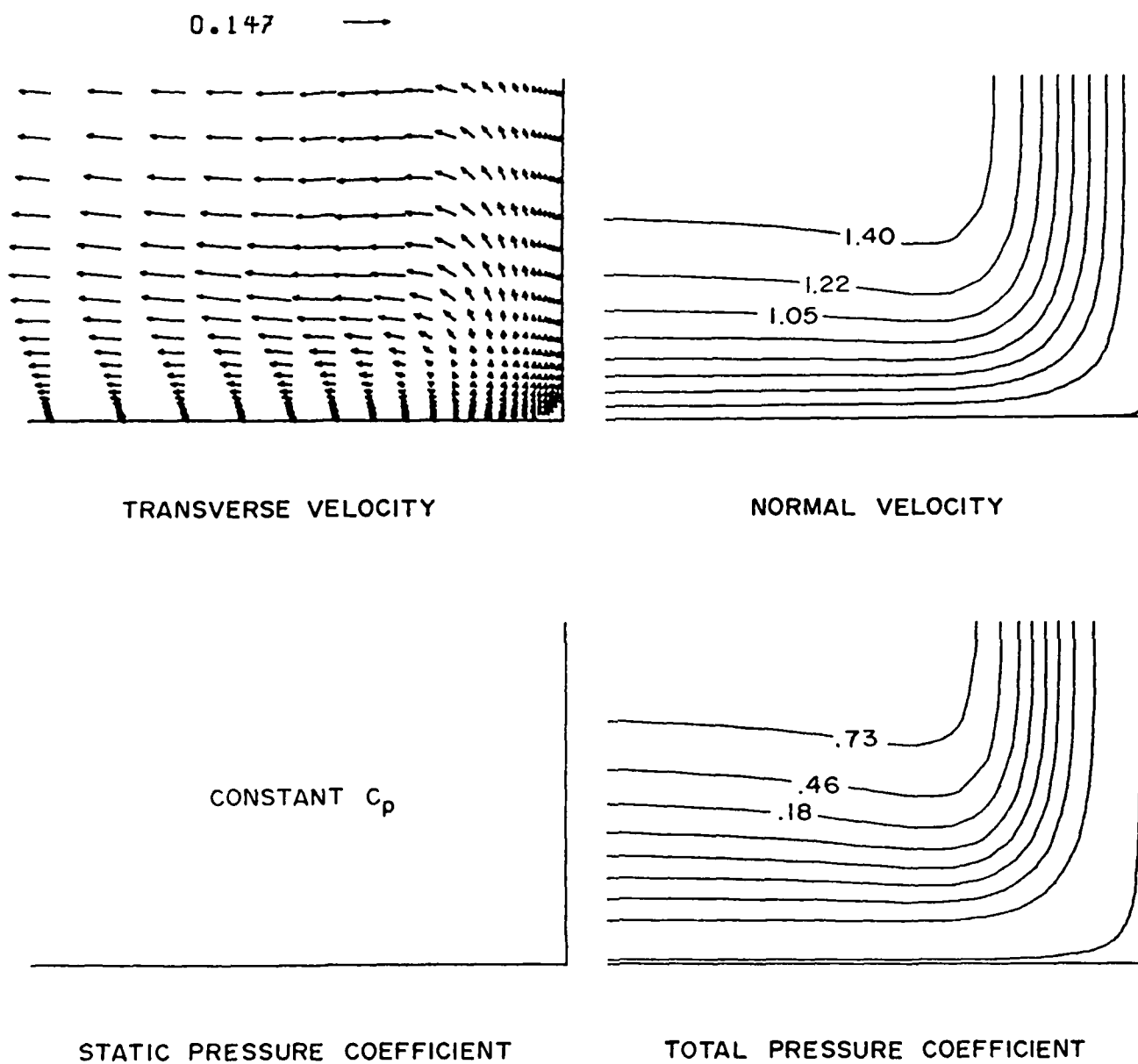STATIC PRESSURE COEFFICIENT

TOTAL PRESSURE COEFFICIENT

Fig. 9f – Computed Flow Variables in Plane 6.

END

FILMED

2-85

DTIC